Investigation of water jet breakup behavior in crossflow with a supersonic air jet

H. J. Jones[1*], S. K. Menon[2]

[1]Graduate Research Assistant, Mechanical & Industrial Engineering, Louisiana State University, United States

[2]Assistant Professor, Mechanical & Industrial Engineering, Louisiana State University, United States

Abstract

In the testing of rocket engines, it becomes very important to protect the testing hardware from damage by the extreme thermal and acoustic loading generated by the high-energy rocket exhaust. To better inform the testing hardware development at NASA's Stennis Space Center in Mississippi a complex multi-phase CFD code has been developed to inform the design of water spray systems used to cool rocket exhaust and mitigate the effects of acoustic loads. To assist in the validation of this computational code, a scaled test facility has been developed at Louisiana State University to examine the behavior of a representative water jet breakup interaction with a supersonic jet of air. A 0.38" diameter air jet of Mach number 2.8 and stagnation pressure of 150 psig interacts with a 0.06" diameter water jet at a pressure between 0-100psig, and non-intrusive diagnostics are used to examine the breakup process and behavior. A laser sheet is used to visualize the breakup of the jet in-plane with both the water and air jets, and the breakup process and stability are analyzed.

Keywords: jet in crossflow, shockwave interactions, cooling applications, imaging diagnostics

Introduction

Beginning in the early 1960's with NASA's Apollo program, Stennis Space Center (SSC) was built as a remote facility for developing rocket engines. Since then the center has grown to accommodate the testing of not only the newer engines used for the Space Shuttle program and NASA's Space Launch System (SLS) currently in development, but also serves as a testing facility for NASA's commercial partners including SpaceX, Blue Origin, Aerojet Rocketdyne, and Orbital Sciences. The test facilities at SSC must be protected from damage from the high temperature, high energy exhaust gases which these rocket engines generate, as well as the massive vibrations which can be generated due to acoustic loads. Figure 1 (*left*) shows a large-scale test of the RS-68 engine. These destructive forces are mitigated using water injection systems which serve the dual purpose of both cooling the exhaust and allowing it to be reliably carried away by a flame trench or deflector, as well as serving to break up the turbulent eddies around the exhaust which transmit much of the engine's acoustic energy. In the absence of water injection systems, the flame trench can sustain damage as seen in Figure 1 (*middle*) which shows a photograph of an uncooled trench following a test firing of an AJ26 engine. Issues including degradation and ejection of flame deflector material during testing are observed along the trench wall. Such effects can be mitigated by using water sprays as shown in Figure 1 (*right*) which shows a cooling ring in action during static testing of the engine used on NASA's Morpheus lander.

Figure 1: Left: Large scale test stand during test firing [2]; Middle: Damage caused to uncooled flame trench, NASA SSC. April 26, 2017; Right: Water spray ring used to cool Morpheus engine static tests [1]

While the case-by-case engineering that is done for many of the subscale tests completed is done in an effort to minimize the material and facility cost for each test, the analysis performed for the tests on the large scale stands is completed with the goal of minimizing the required water output into the perforated flame trench that the stand is equipped with. The large scale test stands at SSC can deliver cooling water flowrates in excess of 300,000 GPM, and should the requirement for water suppression flowrate be minimized for each test on the stand the facility requirements for pump size and wear on these large pumps can be decreased, decreasing overall costs.

In an effort to optimize the water cooling systems, recent work at SSC has focused on the development of computational capabilities to model the exhaust plume cooling configuration using a tightly-coupled multi-phase computational framework. Figure 2 shows results from the numerical simulation including an overlay of the simulation results on the actual deflector plate after rocket tests to correlate component damage to the modeling results. The figure shows temperature and droplet cloud iso-intensity contours separately and overlaid on each other for a case where water injection is carried out into a rocket exhaust plume. As can be seen, the results agree quite well on this scale with the simulation results properly predicting the highest temperature at the plume impact points and showing areas of the plate with lower levels of cooling water coverage to be exposed to higher temperatures.
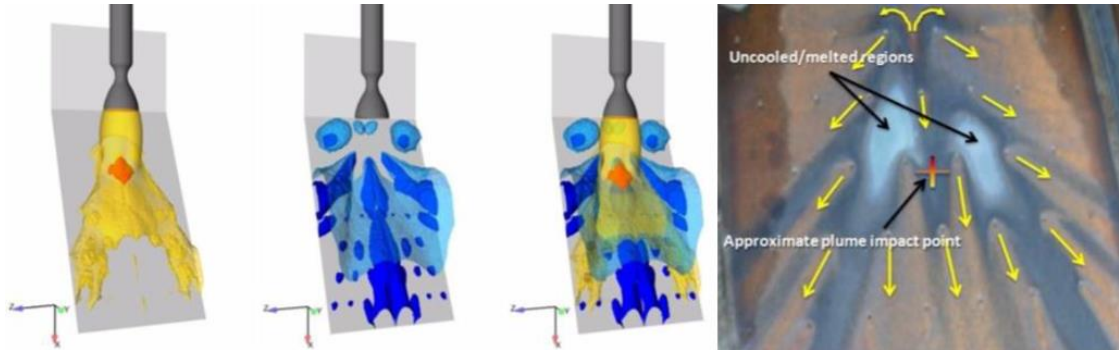

Figure 2: Left: separated gas and liquid phase, combined CFD results; Right: Deflector plate after experimental test [3]

Though there is promise of agreement in the macro-scale, the complexity and large parameter space present in the actual systems necessitates experimental validation on a smaller scale. Additionally, a scaled experimental setup with appropriate diagnostics will make it possible to provide information that could enable further optimization of the water spray approach followed in the full scale tests at SSC. As mentioned previously, the chief objectives of the water spray are to achieve cooling (of the deflector plate and the exhaust plume) and to suppress noise. A scaled experimental setup makes it possible to investigate the parameters potentially having a strong impact on the optimization of the water spray approach including the location of water injection (both within the shock structure as well as at different locations downstream of the nozzle exit) and water injection pressure.
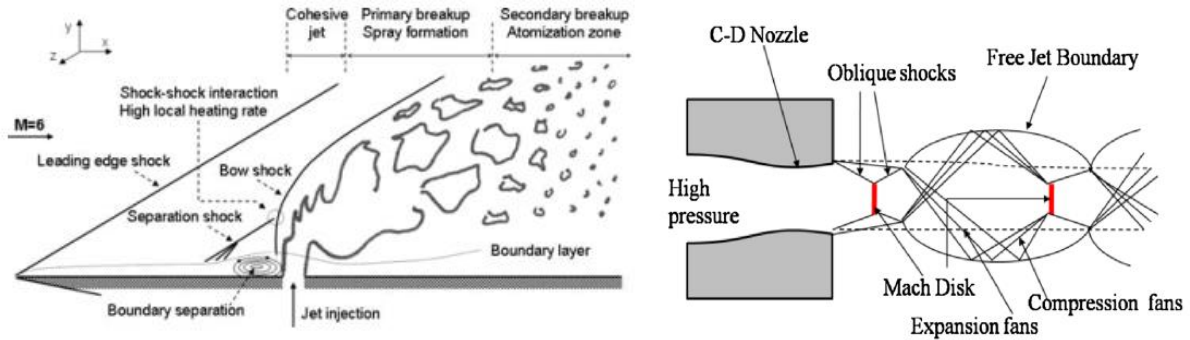

Figure 3: Left: Shock structure for jet-in-crossflow configuration [4]; Right: Structure of an overexpanded free jet [5].

Separate from the issue of code validation, the structure of the water jet impacting a supersonic plume could result in a markedly different spray breakup as opposed to the injection of a liquid jet into a supersonic crossflow of gas through a boundary layer. The latter problem has been studied extensively in the past due to its relevance to fuel injection in scramjet engines and other related configurations and yields a shockwave structure as shown in Figure 3 (*left*). For the conventional jet injected into a supersonic crossflow as shown in Figure 3, the adverse pressure gradient caused by the injection of the liquid jet results in the separation of the boundary layer and the formation of a separation shock. Figure 3 (*right*) shows the structure of an overexpanded free jet [5] similar to the one studied in this work. Understanding the injection of a liquid jet into this flow is of fundamental importance, both from the perspective of how the shock structure is modified by the presence of the water jet as well as how the water spray structure forms from the interacting jets. The key difference between the canonical jet in crossflow and the problem at hand is the absence of a solid boundary at the liquid injection point.

Following the motivation as described above, this work utilizes an experimental approach to study the interaction of a water jet into a supersonic free jet. The supersonic jet is formed by the expansion of room temperature air through an overexpanded nozzle. The current work forms a precursor to a "hot flow" investigation, which will utilize a scaled hybrid rocket setup to generate a hot supersonic free jet. The experimental test setup is described next along with the various diagnostic tools that are utilized in this work to visualize the supersonic flow structure

2

as well as the impinging water jet, which results in a spray structure. Next, the test conditions of interest are laid out with respect to the water injection pressure and the corresponding liquid to gas momentum flux ratio. Non-dimensional numbers relevant to this work are calculated to locate the current test conditions within the regime of jet breakup processes which have been studied previously. Next, results are presented showing the water jet interaction with the supersonic air jet. A qualitative structure of the flow as well as quantitative results showing the mean flow path of the water jet are presented. Finally, the resulting water spray is analyzed quantitatively using Principle Orthogonal Decomposition (POD). Following a discussion of the results, conclusions and future research directs are presented.

Experimental Methods

Figure 4 (*left*) shows a schematic of the test stand used in this work. It is designed to act as a platform which will allow for the investigation of the current cold gas flow configuration as well as combusting flows to be used in future work. A compressor supplies high pressure air which is regulated down to 120 psig and supplied to a converging diverging (C-D) nozzle. The nozzle has an exit diameter of 9.65 mm (0.38") and an area ratio of 2.25. Air expansion through the nozzle results in a Mach 2.8 gas flow at the exit. The flow is overexpanded and results in a structure similar to that shown schematically in Figure 3. A pressurized water jet is generated using the same air supply, which can provide liquid injection pressure of up to 150 psi. The pressurized water is delivered to a nozzle of 1.524 mm (0.06") diameter, which produces the water jet. Figure 4 (*right*) shows a photograph of the water injection nozzle as well as the exit plane of the C-D nozzle for air. The liquid jet is mounted on a traverse, which allows for variation in the injection location downstream of the nozzle exit and the angle at which the liquid is injected. The air pressure is monitored using a pressure gauge mounted at the chamber inlet. Water pressure is monitored using a digital pressure sensor upstream of the nozzle. Air and water temperatures are monitored using K-type thermocouples. A totalizing water flow meter is also installed to measure the flow rate through the nozzle.
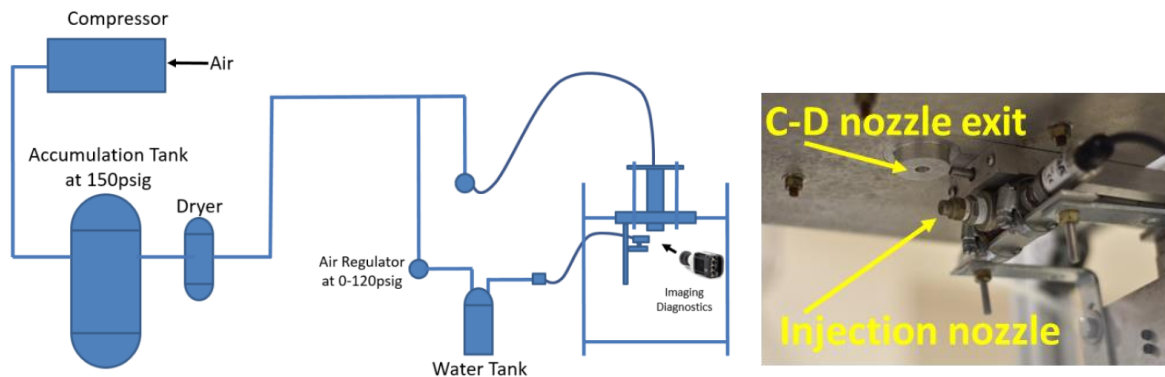

Figure 4: Left: Cold flow experimental diagram; Right: Photograph of the water injection system.

A novel Focusing Color Schlieren (FCS) system is used to examine the shock wave structure in the flow exiting the nozzle and modifications to it caused by liquid injection. The FCS technique replaces the source grid in a traditional focusing Schlieren with a color-coded source image. The cutoff grid is replaced by a two-dimensional cutoff. The focusing Schlieren technique [6] itself is an improvement over the classical Schlieren system which uses light collimated by optics such as mirror or lenses. The current implementation of the FCS technique allows for detection of directionality in the gas flow as well as an ability to focus on a specific thin section of the measurement section; allowing for axisymmetric examination of flow behavior at a specified location. Figure 5 shows a schematic of the color FCS techniques and a detailed description of the setup can be found in the work by Schoegl et al. [7].

The breakup process of the water jet post injection into the air jet is visualized using a high-speed camera (Photron FASTCAM). Illumination by a continuous laser sheet aids in evaluation of liquid structure while imaging with the FCS system while volume illumination using a single 500W halogen bulb is used to examine liquid behavior during high speed imaging. The laser sheet used in illuminating the water spray is obtained from a SpectraPhysics Stabilite 5W laser with a 2 mm beam. The high-speed images are examined visually for breakup characteristics and are also post-processed using proper orthogonal decomposition (POD) to reveal characteristic breakup modes in the turbulent process that can reveal the driving mechanisms of breakup [8].
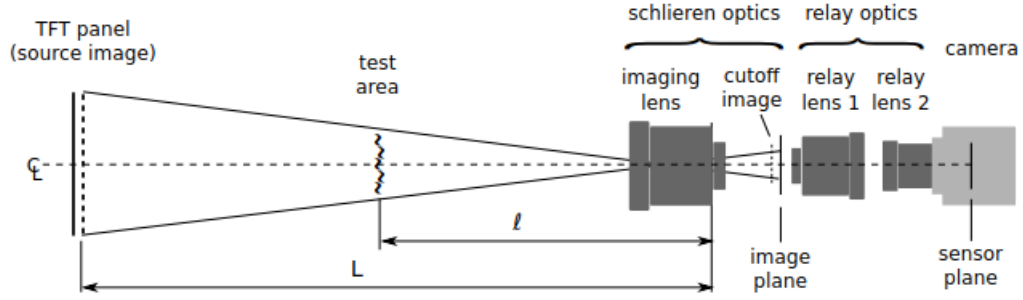
Figure 5: Schematic of the focusing color Schlieren image as employed in the current work [7].

Based on the range of possible injection pressures, the water flow rate can be varied. The total air pressure at the inlet to the chamber is maintained at 150 psig for all test cases. For the corresponding air density (ρ_g) of 13.4 kg/m^3, air velocity at the nozzle exit is calculated as $u_{inf} = 608$ m/s. The water jet exit diameter, d_o, is 1.524 mm. There are a few non-dimensional groups, which can be used to compare the physical effects contributing to the breakup process. The non-dimensional groups can be calculated using the above parameters and properties of water including surface tension ($\sigma = .07197$ N/m), dynamic viscosity ($\mu_l = 1$ $mPa \cdot s$), and density ($\rho_l = 1000$ kg/m^3). The gas Weber (We_G) number is given by,

$$We_G = \frac{\rho_g u_{inf}^2 d_o}{\sigma}$$

and is used to examine the relative effects of the inertial contribution of the gas flow and the surface tension forces which stabilize the liquid flow. The Ohnesorge (Oh) number is given by,

$$Oh = \frac{\mu_l}{(\rho_l d_o \sigma)^{\frac{1}{2}}}$$

and compares viscous forces to inertial and surface tension forces in the liquid. The momentum ratio (q) compares the energy present in the liquid and gaseous phases and can be used to locate the current test cases within regimes established for liquid jet breakup processes. The momentum ratio is given by,

$$q = \frac{\rho_l V_{jet}^2}{\rho_g u_{inf}^2}$$

where V_{jet} is the water jet exit velocity. Finally, the liquid jet Reynolds number (Re_l) is given by,

$$Re_l = \frac{\rho_l d_0 V_{jet}}{\mu_l}$$

Calculations using the above equations results in an Ohnesorge number of $Oh = 0.0003019$ and a corresponding gas Weber number of $We_G = 102{,}290$ for all cases. The liquid jet velocity, momentum ratio, and Reynolds number are shown in Table 1 for the different water injection pressures studied in this work.

Table 1: Operating parameters for water corresponding to the different injection test cases

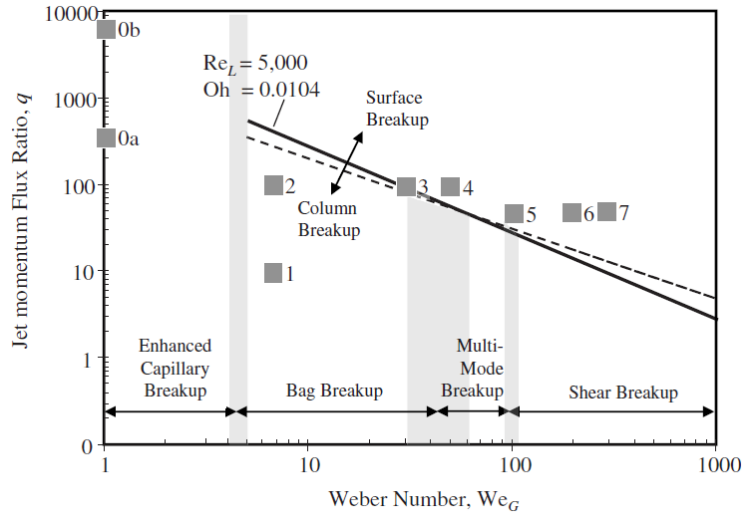| Injection pressure [psig]	Jet speed, V_{jet} [m/s]	Momentum ratio, q	Reynolds number, Re_l
20	4.38	0.00397	6678
40	8.76	0.0159	13,355
60	13.14	0.0358	20,032
80	17.53	0.0636	26,710
100	12.91	0.0993	33,388

Figure 6: Regimes of liquid breakup processes [8]

Based on the gas Weber number and the momentum ratio, various regimes of liquid breakup processes in gas crossflow have been identified [8] as shown in Figure 6. Figure 6 can be used to locate the test conditions of the current work with respect to the various liquid breakup processes explored in literature. As can be seen, the gas Weber number investigated in this work is almost an order of magnitude higher than the range illustrated in Figure 6. Further, the current tests are performed at a very low momentum flux ratio given the large air jet velocity exiting the nozzle

Results and Discussion
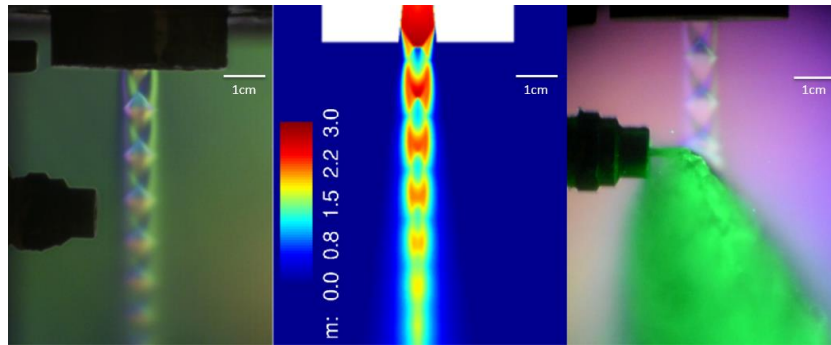
Shock structure imaging

Figure 7: Left: Preliminary FCS image, Middle: Corresponding CFD Mach number contour plot; Right: FCS image with continuous laser sheet liquid illumination

To validate the design of the cold flow chamber, FCS was used to examine a baseline shockwave structure in the gas phase. Figure 7 (*left*) shows an image of the shock structure produced by the overexpanded air jet leaving the nozzle at a design Mach number of about 2.8. Figure 7 (*middle*) shows iso-contours of the Mach number calculated using a CFD code for the same operating conditions and nozzle geometry. Qualitatively, good agreement is seen in the shockwave structure with respect to the number of 'cells' or Mach diamonds in the shock train, their spacing, and their size. A continuous laser sheet was also used to examine the liquid flow structure. Images of the laser sheet were acquired at 60 fps on a traditional DSLR camera. Figure 7 (*right*) shows one such image for a case with a water injection pressure of 80 psig. For this case, the momentum ratio, q, is 0.0636, high enough for the water jet to completely penetrate the air jet. Upon closer inspection, a shock wave that was not present in the free air jet is observed slightly upstream of the location where the water jet impinges upon the air jet. The shock train structure upstream of this newly created shock wave does not appear to be affected by the water injection process. The water jet is completely broken up to produce a spray. The DSLR image captures a time-averaged spray structure as shown in Figure 7 (*right*). Video images of the phenomena show some recirculation patterns towards the leading edge of the spray. Overall the spray appears to be highly turbulent in nature. Next, we examine the effects of varying the jet injection location and momentum ratio.

Effect of jet injection location

Figure 8: Shock structure interaction for varied injection location

Figure 8 shows results from FCS imaging of the shock structure and laser sheet imaging of the spray for varying water jet injection locations downstream of the air nozzle exit. The momentum ratio is fixed at $q = 0.0636$. The results shown correspond to a liquid injection angle of 90°. The bottom row of images in Figure 8 are zoomed in versions of the images in the top row for closer inspection. The three images in Figure 8 roughly correspond to water injection: between the 2nd and 3rd Mach diamonds in the shock train, almost directly into the oblique shock waves for the 3rd Mach diamond in the shock train, and just below the oblique shocks of the 3rd Mach diamond in the shock train. In all three cases, the images show the presence of a strong bow shock at the liquid gas interface. However, the separation shock present in traditional jet in crossflow as seen in Figure 3 is not observed. Note that the leading edge shock seen in Figure 3 is caused by the leading edge of the flat plate used in that experiment and should not be expected in this work. The presence of stationary Mach diamonds in this over-expanded gas flow yields some further interesting characteristics not evident in traditional confined supersonic jet in crossflow experiments. For the middle image in Figure 8, the bow shock directly interacts and appears to merge with the forward oblique shock waves for the 3rd Mach diamond. For the right image in Figure 8, a flattening of the forward oblique shockwaves occurs as they are forced to follow the contour of the bow shock produced upstream of the water jet. The bow shock itself, which is formed near the liquid boundary after the liquid jet injection point enters the expansion region rear of the Mach diamonds is weakened due to the presence of the upstream shock waves. This general behaviour is exhibited for water injection near each successive Mach diamond with further downstream interactions resulting in weaker shockwaves as total pressure present in the gas flow decreases due to viscous dissipation.
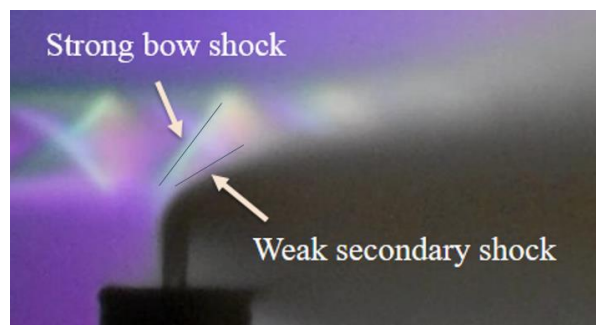
Effect of momentum ratio

Figure 9: Shockwave structure for low momentum ratio q=0.002

Next, the effect of varying the momentum ratio is examined. Figure 9 shows the shockwave structure for a low momentum ratio of $q = 0.002$. In this case, the water jet does not completely penetrate the air jet as is the case in the images shown in Figure 8. The bow shock which is observed in the previous images is once again observed near the leading edge of the liquid jet. However, an additional weak boundary shock wave is seen between the bow shock and the liquid interface which was not observed for the high momentum ratio case. Parts of the Mach diamonds downstream of the injection location are still visible in the images shown in Figure 9, but are considerably blurred presumably due to the spray mist of water formed in the field of view. No separation shocks as observed in Figure 3 for the traditional jet in supersonic crossflow is observed. The separation shock in Figure 3 is primarily a result of the adverse pressure gradient resulting in the separation of the boundary layer. The

boundary layer in that case is formed by the flow moving over the flat plate leading up to the liquid injection point. In the current setup, the free jet boundary acts similar to the flat plate boundary. But this boundary behaves more as a shear layer than a flat plate induced boundary layer. Hence no separation effects are observed in the current configuration.

In addition to the jet interaction phenomena, it is useful to examine the penetration of the liquid jet into the air jet for varying momentum ratios. Further, the experimental results can be compared with values predicted by an analytical formulation by Yates [9], which was used in the initial sizing and choice of the test cases. Figure 10 shows the liquid jet penetration distance as a function of downstream location for four different water injection pressures. The solid lines represent experimental data while the dashed lines correspond to Yates' correlation. The penetration height for the liquid jet is extracted from the images as the path corresponding to iso-intensity contour peaks along the mean flow path. Figure 11 (*left*) shows a representative mean intensity image for 15,000 frames used to compute such a path. As expected, the penetration height increases with the water injection pressure. The analytical results predict a higher penetration height as compared to the experimental results. This is presumably due to the excess energy required for the liquid jet to penetrate the highly viscous layer between the ambient air and potential core of the gas jet.
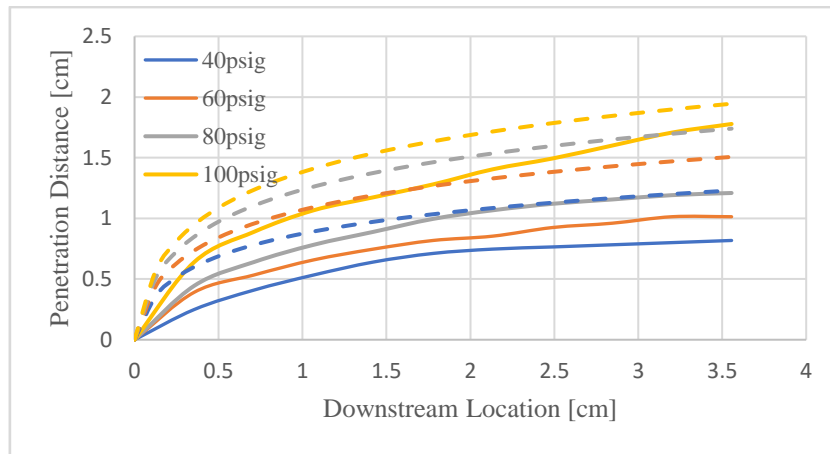

Figure 10: Liquid jet penetration distance for varied injection pressure

To further examine the complex behavior of the turbulent jet breakup process, a Principle Orthogonal Decomposition (POD) analysis is performed. The objective of the POD analysis is to capture coherent spatial modes which capture a significant proportion of the image intensity fluctuations. Analysis of the spatial modes can reveal their contribution the spatial development of the overall jet. The POD analysis is carried out in this work using high speed images of the water jet breakup obtained using a high speed camera. The POD method applied to fluid flow images is similar to the analysis carried out by Arienti et al. [9] and is not included here for brevity. Figure 12 shows snapshots of the water jet breakup at the exit of the nozzle corresponding to three cases of increasing momentum ratios: 0.00397, 0.0159, and 0.0636. For increasing momentum ratios, a transition is observed from shear breakup for low momentum ratio to surface breakup at higher momentum ratios, which is consistent with the behavior shown by Arienti et al. [9]. The POD analysis was applied to the results for a momentum ratio of 0.0636. A series of 15,000 images were used in the analysis and correspond to a time interval of 750 ms during which a quasi-steady behavior was observed in the experiment. Figure 11 shows the 3rd and 4th proper orthogonal modes (POMs) at q=0.0636 taken at a frame rate of 20,000fps along with the ϕ_0 mode representing a pixel intensity average for the test case. Flapping and bending modes are observed similar to what was seen for the surface breakup phenomena examined by Arienti et al [8]. This behavior is expected due to the high gas Weber number We_G, and is to be explored as a means of quantifying breakup behavior. These behaviors are to be characterized further but have thus far been consistent in general with what is present in a more traditional jet in cross flow configuration.
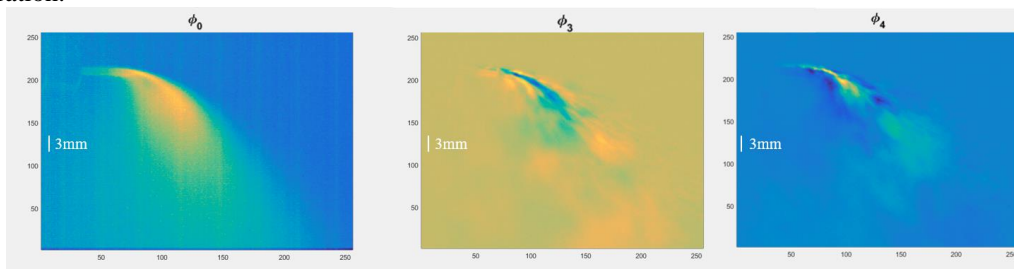
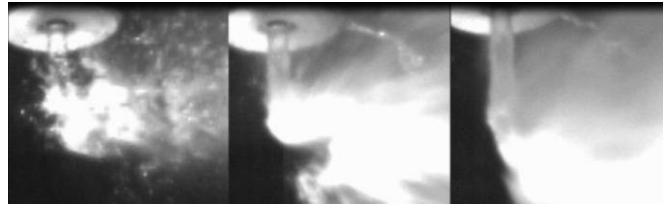*Figure 11: 3rd and 4th proper orthogonal modes (POMs) for q=0.0636*

Figure 12: Volume illuminated high speed snapshots for q=0.00397, q=0.0159, q=0.0636

Summary and Conclusions

The interaction of a water jet impinging upon an overexpanded supersonic free jet of air has been investigated using experimental methods. This phenomenon is relevant to water spray cooling of rocket engine exhaust plumes to reduce thermal and acoustic loading. Parametric studies were conducted varying water injection pressure and injection location. Focusing color Schlieren was used to visualize the shock structure while high speed imaging using laser sheet and volume illumination were used to image the water jet and spray structures. A bow shock is formed at the leading edge of the injected jet for all the cases investigated. The shock structure upstream of the injection is unchanged while the water jet itself breaks up into a turbulent spray. Depending on the injection location with respect to the Mach diamonds in the shock train, the bow shock is seen to modify the oblique shocks resulting in an increase in the included angle between the shock waves. Varying the momentum ratio by changing the water injection pressure is seen to change the penetration height of the water jet in accordance with correlations developed for a traditional jet in supersonic crossflow. However, the penetration height is seen to be lower for the current case due to the requirement for the water jet to push through the jet boundary to reach the core flow. Increasing the momentum ratio is also seen to change the jet breakup process going from a shear breakup mode at low momentum ratio to a surface breakup at high ratios. This is in agreement with breakup modes observed for jet in crossflow configurations and corresponds to the gas Weber number and momentum ratios for the present configuration. Finally, a POD analysis utilizing high speed images allows for the separation of the jet breakup processes into coherent spatial modes. Flapping and bending modes are seen to be the dominant modes for high momentum ratio flow conditions corresponding to a surface breakup phenomenon. Future work will extend the POD analysis to other flow conditions. Phase Doppler Particle Anemometry will also be utilized to quantitatively measure spray properties including droplet size and velocity distributions. The comprehensive experimental dataset will be utilized to validate numerical simulations of the experiment performed using a multi-physics code by collaborators at NASA Stennis.

Acknowledgements

References

[1] Project Morpheus. (n.d.). Retrieved January 4, 2018, from https://en.wikipedia.org/wiki/Project_Morpheus

[2] RS-68 Engine. (n.d.). Retrieved January 4, 2018, from http://www.rocket.com/rs-68-engine

[3] Sachdev, J. S., Ahuja, V., Hosangadi, A., & Allgood, D. C., *46th AIAA/ASME/SAE/ASEE Joint Propulsion Conference & Exhibit*, Nashville, Tennessee, July 25-28, 2010.

[4] Liu, H., Guo, Y., & Lin, W., *Advances in Mechanical Engineering* 8: (2016).

[5] Shelar, V. M., Rao, S., Hegde, G. M., Umesh, G., Jagadeesh, G., & Reddy, K. P. J., *International Journal of Mechanical and Materials Engineering* 9: p. 28 (2014).

[6] Burton, R.A., *J. Opt. Soc. Am.* 39: 907-908 (1949).

[7] Schoegl, I., Pisano, A. J., & Sedky, G., *54th AIAA aerospace sciences meeting*, San Diego, CA, USA, 2016.

[8] Arienti, M., & Soteriou, M. C., *Physics of Fluids* 21: (2009).

[9] Yates, C. L., Technical Report AFAPL-TR-71-97: (1972).